Decompression Effects on Suppurative and Sclerosing Osteomyelitis in the Jaw

Buyanbileg Sodnom-Ish
Seoul National University
Mi Young Eo
Seoul National University
Ji Hye Oh
Seoul National University
Mi Hyun Seo
Seoul National University
Hoon Joo Yang
Seoul National University
Jong Ho Lee
Seoul National University
Soung Min Kim (smin5@snu.ac.kr)
Seoul National University

Research Article

Keywords: Osteomyelitis of jaw, Staphylococcus aureus, decompression, micro-CT, immunohistochemistry (IHC)

Posted Date: March 5th, 2021

DOI: https://doi.org/10.21203/rs.3.rs-235248/v1

Abstract

Background: Osteomyelitis (OM) of the jaw is usually caused by a chronic odontogenic infection. Decompression is the release the intraluminal pressure in the cystic cavity allowing gradual bone growth from the periphery. The aim of this study was to analyze the effectiveness of decompression in an OM jaw model.

Methods: A 4-mm-diameter defect was made on mandibles of fourteen Sprague-Dawley rats and inoculated with *S. aureus* (20 µl of $1x10^7$ CFU/ml) injection. Two weeks later, four groups were made as non-treatment (C1), only curettage (C2), curettage and decompression (E1), and curettage and decompression with normal saline irrigation (E2). After four weeks, each group was analyzed.

Results: Most micro-CT parameters of C1 and C2 were significantly lower, and bone mineral density with bone volume was enhanced in E2. E1 and E2 groups in histology showed prominent bone healing with a significantly high number of osteocytes, E2 had the weakest expression of IL-6 compared to that of C1. TNF-α and OPN were expressed strongly in the E1.

Conclusion: Decompression drains induced advanced bone healing compared to that of curettage alone in an OM jaw model. Therefore, it could be recommended to use decompressive drain for the enhancement of jaw OM management.

1. Introduction

Osteomyelitis (OM) of the jaw is an inflammatory process that starts in the medullary space of the bone and progresses to cortical bone, the Haversian system, periosteum, and overlying soft tissue. This is usually caused by micro-organism infection into the bone tissues due to a trauma or odontogenic infection[1]. The gram positive pathogen *Staphylococcus aureus* (*S. aureus*) is the most common OM causative agent in both children and adults[2]. Other reasons include steroids, chemotherapeutic drugs, and bisphosphonates, which have been linked to jaw OM[3].

The treatment of jaw OM in the literature is classified as surgical and non-surgical, while the aim differs depending whether or not bacterial infection is apparent[4]. The universally acknowledged and effectual treatment is a combination of antibiotic therapy and surgery consisting of sequestrectomy, saucerization, decortication, and closed-wound suction irrigation[5]. The surgical therapy approach has three main goals, which includes decompression and drainage of intramedullary pressure and subperiosteal abscesses caused by the osteomyelitic effect, surgical treatment of infected tissue and removal of infectious foci, and grafting healthy bone tissue into the infected area[6].

By definition, decompression is a technique that creates a small opening in the cystic wall for drainage that releases intraluminal pressure that causes cystic reduction and permits gradual bone growth from the periphery. This technique has been associated with minimal surgical morbidity, changes in the malignancy environment, prevention of reestablishment of intraluminal pressure, decrease or inhibition of

the expression of interleukin (IL) 1α and IL-6 inside odontogenic cysts, maintenance of pulp vitality, preservation of anatomical structures, prevention of pathologic fracture, thickening of the cystic lining, and relatively low risk of recurrence[7].

Surgical drains are used for decompression effects, to eliminate pooled blood, serum and edema reduction, exudate management, and dead space reduction of the surgical wound by drawing the separated surfaces together[8]. These interventions are classified as open and closed with the closed one subdivided as passive or active. Active negative pressure drainage, also known as vacuum-assisted wound closure or negative-pressure wound therapy is a popular method for wound care including limb wounds, soft-tissue defects, chronic OM, osteofascial compartment syndrome, amputation, and replantation. Past research results have shown the effects of using negative pressure wound therapy in the head and neck region that include decreased healing time, less pain, and full drainage effects[9]. Despite the increasing number of studies of decompression, there are no reported studies of decompressive effects using drains in the management of jaw OM.

The hypothesis of this study was that decompression is more effective with regard to bone healing for the treatment of jaw OM compared with conventional surgical treatment alone. The purpose of this study was to investigate the effectiveness of decompression using a drain compared to management without drainage in a rat model of *S. aureus*-induced OM using micro-computed tomography (micro-CT) and histopathological analysis.

2. Materials And Methods

2.1 Establishment of an *S. aureus*-infected jaw osteomyelitis rat model

Fourteen 8-week-old SPF Sprague-Dawley rats (OrientBio Inc., Seongnam, Korea) weighing 230.13 ± 13.87 g on average were used in our study. The experimental protocols were approved by the Seoul National University (SNU) Institutional Animal Care and Use Committee (SNU-121123-12-11) and Institutional Biosafety Committee of SNU (SNUIBC-R121226-1-6). The experiment was in accordance with the “Recommendations for handling of Laboratory Animals for Biomedical Research” and complied with the Committee on Safety and ethical Handling Regulations for Laboratory Experiments at SNU. Animal studies were conducted following the ARRIVE guidelines for animal research[10]. The animal experiment was conducted at the Institute for Experimental Animals, College of Medicine, SNU, in a laboratory infection room classified as for high risk infection studies or infectious studies that use experimental animals (Animal Biosafety Level 2: ABL 2). All animals were maintained in an individually ventilated 12-hour light/dark cycle cage system with the temperature ranging from 20–26°C (23 ± 3°C), and were provided rodent food and water ad libitum.

The bacterial strain used in our study was *S. aureus*, the most common causative pathogen for jaw OM[11]. We used a 2°C to 8°C freeze-dried *S. aureus* subsp. *Aureus* (ATCC® 29213, Manassas, VA, USA) and a

Wichita designated clinical isolate that was provided by the Korean Culture Center of Microorganisms (KCCM®, Seoul, Korea).

The suspended sample containing the *S. aureus* strain was then inoculated and spread with the spread method into a tryptic soy agar (TSA, BD Difco™, New Jersey, USA) plate medium using a sterilized inoculation loop and cultured in an incubator for 24 hours at 37°C. After incubation, a visible colony of *S. aureus* formed. To determine bacterial density, we used the direct method of plate count technique (PCT) and the indirect method of turbidometry[12]. The number of bacterial inoculation was determined by PCT, in which the number of colonies formed on the plate medium is proportional to the live bacteria contained in the sample, and the dilution ratio and the number of colonies are calculated by stepwise dilutions.

In the turbidity measurement, as the concentration of bacteria increases, the turbidity (absorbance) increases proportionally, therefore in order to measure turbidity as the actual number of bacteria, a correlation must be obtained. This can be obtained by measuring the number of bacteria with the direct plate count technique in parallel. The bacterial colony was harvested and was washed two times with 1 x PBS by vortexing and by centrifuge. The suspended *S. aureus* solution was transferred to a new glass cuvette containing 1xPBS and was adjusted to an optical density (OD) of 0.8 using a UV/VIS spectrophotometer (Spectrophotometer, PerkinElmer®, MA, USA) at 600 nm with a clear PBS solution as a control (Fig. 1A). For the study, the TSA culture was diluted by 4 different OD values in four steps: (OD = 0.2) 1.1X10□; (OD = 0.4) 2.0X10□; (OD = 0.6) 4.5X10□; (OD = 0.8) 1.1X10□. The bacterial inoculation was then determined to be (600 nm = OD0.8) 1x10□ CFU/ml, as the optimal bacterial amount required to induce jaw OM.

The infection with *S. aureus* was performed using a local inoculation route by injecting the bacterial suspension through the created defect[12]. The inoculation procedure was performed under general anesthesia using 90 mg/kg ketamine (50 mg/ml) (ketamine hydrochloride®; Yuhan Co., Seoul, Korea) + 10 mg/kg xylazine (23.32 mg/ml) (Rompun®; Bayer Korea, Ansan, Korea) that was administered intraperitoneally. The preparations for the surgical procedure including the skin preparation, disinfection, and draping were all performed according to standard protocols (Fig. 1B). An approximately 12 mm full-thickness longitudinal extra-oral incision was made parallel to the inferior border of the right and left side of rat mandibles. Adequate subcutaneous (Fig. 1C), deep fascial and periosteal dissections were performed followed by retraction with forceps (Fig. 1D). Using a low-speed hand piece with 1.2 mm diameter round bur, a bilateral circular 4 mm defect was created in the rat mandible (Fig. 1E) with copious irrigation. The defect was made from the buccal side, inferior to the incisor tooth root, posterior to the second molar, and at the attachment site of the superficial masseter muscle. Considering the anatomy of the rat and the objective of the study, a circular 4 mm defect is a generally accepted mandibular bone defect[13].

All animals received 20 µl of 10^7 CFU/ml *S. aureus* injection (Fig. 1F) into the defect and were covered with Greenplast kit® fibrin glue (Greencross Co., Yongin, Korea) (Fig. 1G). The surgical wound was then carefully sutured at the subcutaneous layer with resorbable 4 − 0 Vicryl® (Polyglactin 910®, Johnson &

Johnson Co., NJ, USA) sutures and the skin closure was performed using silk sutures (Black silk®, 2–0; AILEE Co., Busan, Korea) (Fig. 1H).

2.2 Grouping and experimental design

The animals were randomly divided into control (non-decompression groups, C1 and C2) and experimental groups (decompression groups, E1 and E2) (Table 1). The C1 group (n = 3) served as the control group, who only received wound closure. The C2 control group (n = 4) received conventional surgical curettage for jaw OM.

Table 1
Animal grouping. The animals were divided into control groups (C1 and C2) and experimental groups (E1 and E2).

Group	Treatment	Sacrifice period
C1	Non-decompression group, suturing after incision	4 weeks
C2	Non-decompression group, debridement of necrotic tissue and curettage	4 weeks
E1	Debridement of necrotic tissue and draining tube insertion after curettage	4 weeks
E2	Debridement of necrotic tissue and curettage followed by draining tube insertion and normal saline irrigation at 1-week intervals	4 weeks
Abbreviation: CFU: Colony Forming Unit.		

The experimental groups were further classified into two subgroups, E1 group (n = 3), which received removal of pus and necrotic bone tissue and curettage, followed by introducing the tube drain and E2 group (n = 4), which received removal of pus and necrotic bone tissue and curettage, drain insertion and irrigation with normal saline every week.

Blood samples were collected from the tail vein pre-infection, 1-week post-infection, 2-weeks post-infection/the start of the treatment, 1-week after treatment, and 4-weeks after the treatment, and rat weights were checked.

Surgical treatment was performed under general anesthesia as previously described. Two mm inner diameter and three mm outer diameter silicone tubes that were approximately 2 cm in length (Daihan scientific Co. Ltd., Wonju, Korea) were used as a drain. The length of the tube was adjusted to each animal according to the post-curettage conditions and these were sutured in place using 4 − 0 silk sutures. To keep the tubes intact and in place, we used a plastic collar to prevent scratching and accidental displacement of the draining tubes. The animals that died during the experimental trial were recorded for weight loss and clinical symptoms of OM of the jaw.

Upon the completion of the six-week experimental trial, the animals were euthanized by CO_2 inhalation. The mandibles of the rats were immediately harvested and carefully isolated.

2.3 The analysis of bone healing with micro-CT

The rat mandible specimens were subjected to high-resolution micro-CT scanning Skyscan 1172® (Bruker, Kontich, Belgium). The scanning parameters of the source were adjusted to an Al filter of 0.5 mm, source voltage of 70 kV, source current of 141 μA, and 360° rotations at 0.4° rotation steps. This resulted in images that were 496 pixels in width and 900 pixels in height.

Following the scanning procedure, the raw data sets were reconstructed using NRecon 1.6.9.8® (Bruker, Kontich, Belgium) software. The smoothing was adjusted to 6, ring artifact correction to 7, with a beam hardening correction to 10%.

Each dataset was opened and further adjusted using DataViewer® (Bruker, Kontich, Belgium) software. The region of interest (ROI) were determined in the sagittal plane and the image analysis were performed using CTAn software® (version 1.18.4.0, Bruker, Kontich, Belgium). Incisor roots were excluded from the analysis and only bone tissue was included for bone analysis. Equivalent thresholds were adjusted in all images. To determine the ROI, a 4 mm wide circular area was set up in the sagittal plane where the initial 4 mm bone defect area could be seen. For optimal comparison between the samples, an identical number of slices were selected. Four square shaped ROI's were defined as 1.0 mm in width and 1.0 mm in height that were adjusted for analysis at the center and the inferior borders of the circular area as seen in Fig. 2. The same procedure was performed on the contralateral rat mandible. Within the ROI, bone mineral density (BMD, g/cm^3), bone volume (BV, mm^3), and bone volume/volume of interest (BV/VOI, %), bone surface (BS, mm^2), bone surface/volume ratio (BS/BV, 1/mm), trabecular thickness (TB.Th., mm), trabecular number (Tb.N, 1/mm), and trabecular separation (Tb.Sp., mm) were measured and compared. The datasets were reconstructed into three dimensional (3D) images using CTvox volume rendering software® (Bruker MicroCT, Kontich, Belgium).

2.4 The histological and immunohistological analysis of OM healing

The samples from each group were trimmed and decalcified with 0.5 M ethylene diamine tetra-acetic acid EDTA® (pH 8.0) (Biosesang, Seongnam, Korea) solution for ten days, dehydrated with 70% ethanol, and embedded into paraffin. The 4 μm thick slides were then washed with xylene for approximately 10 minutes and were stained with hematoxylin and eosin (H&E) and Masson's trichrome (MT). The histological slides were then scanned with a 3D Scan Panoramic Histech scanner® (3D HistechKft. Budapest, Hungary) and examined using CaseViewer® (version: 2.0, 3DHISTECH, Budapest, Hungary).

For quantitative analysis, the number of osteocytes and Haversian canals within the regenerated bone tissues of the defect area were counted. The 4mm circular defect area was determined from the micro-CT 3D images. An area of interest using a fixed rectangular form of 350 x 300 μm within the initial defect area was established by the histological imaging program CaseViewer® (version: 2.0, 3DHISTECH, Budapest, Hungary) in all of the specimens at a magnification of 20x (Fig. 3).

Paraffin-embedded samples were cut into a thickness of 4 µm and were mounted on glass slides. The examination was performed by using a BX41® Light Microscope (Olympus Co., Tokyo, Japan). For IHC staining we used vascular endothelial growth factor A (VEGF-A) (1:100, ab46154, Abcam, Cambridge, MA, USA), Transforming growth factor β1 (TGF-β1) (1:100, sc-130348, Santa Cruz Biotechnology, Santa Cruz, CA, USA), Osteopontin (OPN) (1:100, sc-73631, Santa Cruz Biotechnology, Santa Cruz, CA, USA), Alkaline Phosphatase (ALP) (1:100, sc-271431, Santa Cruz Biotechnology, Santa Cruz, CA, USA), tumor necrosis factor-α (TNF-α) (1:100, 300-01A, PeproTech, New Jersey, USA) and IL-6 (1:100, sc-28343, Santa Cruz Biotechnology, Santa Cruz, CA, USA) antibodies The staining was scored as follows: “1”: none, “2”: 1–25%, “3”: 26–50%, “4”: 51–75%, and “5”: 76–100% cells stained [14]. The intensity of the antibody staining was assessed using a previously described method [15].

2.5 Statistical analysis

Means and standard deviations for bone healing parameters were obtained. The data normal distribution was tested by Shapiro-Wilk test and showed homogeneity. The differences between groups were tested by ANOVA followed by Tukey–Kramer multiple comparison tests. Statistical analyses were done using SPSS 25.0® (SPSS Software Company, Chicago, USA). $P < 0.05$ were considered statistically significant.

3. Results

3.1 Establishment of an *S. aureus*-infected jaw osteomyelitis rat model

The pathogen dose of 20 µl of 10^7 CFU/ml was effective in creating jaw OM in the rat model and a repeatable animal model was established. After two weeks of infection, all groups showed visible clinical manifestation of infectious jaw OM including: skin redness, swelling, purulent discharge and alopecia. Six animals died after two weeks of infection due to OM complication. Consequently, after six weeks, the specimens of the remaining animals were collected and were further analyzed. All of the animals were in good health before the infection. The clinical findings showed common characteristics of the jaw osteomyelitis. The establishment of *S. aureus*-infected jaw osteomyelitis rat model were confirmed by the following parameters: clinical findings, blood test, micro-CT bone architecture findings, and histological analysis.

3.2 Clinical evaluation with blood test

After the infection with *S. aureus* all animals from the control and the experimental groups showed weight loss. Significant weight loss in all groups was observed with an average of -31.57 ± 21.98 g at one week after the infection that was recovered after two weeks ($p < 0.05$). There was no statistical significance in weight loss between the groups at 1 week after infection

(Table 2).

Table 2
Weight changes after infection with S. *aureus* and treatment in the control and experimental groups.

Group	Before infection (g)	1 week after infection (g)	2 weeks after infection (g)	1 week after treatment (g)	4 week after treatment (g)
C1	223.63 ± 4.12	190.40 ± 11.47	186.63 ± 42.78	211.90 ± 40.58	245.75 ± 4.03
C2	223.35 ± 8.00	177.30 ± 20.30	210.35 ± 25.81	198.40	259.90
E1	246.80 ± 19.47	211.0 ± 5.63	218.17 ± 33.43	243.30 ± 7.07	275.30 ± 19.37
E2	229.27 ± 11.10	216.60 ± 17.41	236.42 ± 20.96	260.46 ± 7.59	294.60 ± 11.51
The weight changes are depicted as mean ± standard deviation (SD).					

The neutrophil count was significantly increased after the infection in all groups. There were no statistically significant differences in neutrophil count between the groups at one week and four weeks after treatment (Table 3). The white blood cell count (WBC) was significantly increased in all groups after infection and was recovered to the normal range at four weeks after treatment. No significant difference was observed between the groups at one week after treatment and four weeks after treatment (Table 4). Serum levels of alkaline phosphatase (ALP) were also measured and analyzed. At one week after infection, ALP levels were significantly increased in all groups and a significant reduction was observed at one week and two weeks after treatment. No significant differences were found between groups (Table 5).

Table 3
The change of the Neutrophil percentage

Group	Before infection	1week after infection	2weeks after infection	1week after treatment	4week after treatment
C1	12.20 ± 3.11	33.45 ± 4.45	29.26 ± 7.82	32.50 ± 3.53	13.00 ± 4.94
C2	28.52 ± 15.13	35.87 ± 19.79	37.00 ± 2.68	29.10	7.90
E1	22.75 ± 15.12	30.36 ± 5.71	20.60 ± 4.10	34.40 ± 9.30	12.77 ± 4.08
E2	16.00 ± 6.29	31.95 ± 2.49	34.12 ± 7.31	28.96 ± 9.00	13.16 ± 2.26
The changes are depicted as mean ± standard deviation (SD).					

Table 4
Changes of WBC count

Group	Before infection	1 week after infection	2 weeks after infection	1 week after treatment	4 week after treatment
C1	8.70 ± 2.74	9.15 ± 3.41	17.10 ± 4.28	16.47 ± 3.73	8.11 ± 1.27
C2	7.51 ± 0.57	12.52 ± 3.05	17.43 ± 9.01	13.37	9.65
E1	12.52 ± 0.67	13.31 ± 3.88	14.63 ± 3.93	16.50 ± 7.02	10.46 ± 1.91
E2	11.19 ± 2.39	17.01 ± 7.61	20.09 ± 3.42	18.38 ± 4.50	11.77 ± 0.62
The changes are depicted as mean ± standard deviation (SD).					

Table 5. Results of ALP changes

Group	Before infection	1 week after infection	2 weeks after infection	1 week after treatment	4 week after treatment
C1	535.33±77.50	957.66±185.30	957.31±957.31	526.00±42.42	389.50±6.36
C2	702.75±107.77	1512.25±267.35	1110.5±272.09	526.00	488.00
E1	817.00±179.67	1374.00±231.63	957.31±213.98	588.00±132.82	407.33± 65.63
E2	739.66±179.66	984.25±302.69	860.00±65.79	718.00±117.20	390.33±101.20

The changes are depicted as mean ± standard deviation (SD).

3.3 Micro-CT results of bone healing

From the 3D images, more bone healing was observed in the E1 and E2 groups, where the initial bone defect was replaced by new bone tissue. The E2 group had the most compact bone formation compared to the other groups. The C1 group, which received no treatment, showed bone destruction that continuously spread from the initial defect affecting a wider area. The common characteristics of osteomyelitis of the jaw such as the bone necrosis and sequestrum formation, a segment of necrotic bone that is separated from the viable bone by a granulation tissue and bone resorption was observed from the control groups.

The BMD results were significantly different between the groups. The BMD in the C1 group was significantly lower compared to that of the E2 group, with a mean difference of -0.45 g/cm^3 ($p < 0.05$) (Table 6) (Fig. 4A).

Table 6
Micro-CT morphometric parameters of the bone regeneration area in 3D analysis

Group	BMD (g/cm^3)	BV (mm^3)	BV/VOI (%)	BS (mm^2)	BS/VOI (1/mm)	Tb.N (1/mm)	Tb.Sp (mm)
C1	0.42 ± 0.27	0.36 ± 0.22	37.31 ± 24.59	5.52 ± 2.42	5.83 ± 2.81	1.51 ± 0.74	0.46 ± 0.19
C2	0.53 ± 0.20	0.47 ± 0.14	46.26 ± 18.19	7.91 ± 1.79	8.04 ± 2.09	2.24 ± 0.53	0.34 ± 0.10
E1	0.70 ± 0.10	0.55 ± 0.08	57.79 ± 19.53	9.80 ± 0.32**	10.70 ± 0.80**	2.78 ± 0.52**	0.17 ± 0.01**
E2	0.87 ± 0.08*	0.73 ± 0.08*	75.70 ± 14.32*	11.07 ± 1.75*	11.44 ± 1.43*	3.28 ± 0.66*	0.12 ± 0.01*
P value	.007	.008	.006	.002	.001	.008	.001

The data is depicted as mean ± standard deviation (SD). Abbreviation: BMD: bone mineral density; BV: bone volume, BV/VOI: bone volume/volume of interest, BS: bone surface, BS/VOI: bone surface/volume of interest ratio, Tb.N: trabecular number, Tb.Sp: trabecular spaces. *$p < 0.05$, E2 group versus the C1 group. **$p < 0.05$, E1 group versus the C1 group.

Table 8
Osteocyte and Haversian canal count in the ROI

Group	Osteocyte	Haversian Canal
C1	60.5 ± 10.1	5.75 ± 3.30
C2	53.5 ± 9.20	8.00 ± 1.40
E1	77.25 ± 8.40	8.50 ± 2.90
E2	91.00 ± 9.90*	9.75 ± 2.10

The data is depicted as mean ± standard deviation (SD). *The osteocytes found in the E2 group were significantly higher than in the C1 and C2 groups, $p < 0.05$).

The BV was highest among E1 and E2 groups. The E2 group showed significantly higher results compared to that of the C1 group ($p < 0.05$) with a mean value of 0.73 ± 0.08 mm^3 ($p < 0.05$) (Fig. 4B). The BV/VOI parameter was significantly higher in the E2 group, with an average value of 75.70 ± 14.32 % compared to that of the C1 group (Fig. 4C). The BS, BS/VOI, Tb.N, Tb.Sp parameters were significantly different between the control and experimental groups (Table 6). Most bone healing parameters were lower in the control groups compared to the experimental groups (Figs. 5A-C). However, the Tb.Sp in the C1 group was significantly higher than that in the experimental groups (Fig. 5D). The Tb.Th was not significantly different between the groups.

3.4 Histological and immunohistochemical results of OM healing

The morphological changes in bone healing were macroscopically observed in the H&E and MT stained slides at 4-weeks in the defect area.

The C1 group showed high grade inflammatory infiltration consisting of neutrophils, eosinophils, and macrophages around the bacterial colonies. Signs of infective osteomyelitis including bone necrosis, bone resorption and destruction, with no bone healing were observed. In MT staining, the C1 group were stained with thick blue color, indicating old bone, while no new bone formation stained with bright blue color were observed (Figs. 6A1-A6). Histological findings for the C2 group showed bone healing with osteoblastic cell lining in the parenchymal tissue found at the center of the defect area with evidence of inflammatory infiltrates (Figs. 6B1-B6).

The histology features of the E1 group included scattered lymphocytic inflammatory infiltrates and loose marrow fibrosis. In the MT stain, new bone formation stained with bright blue color and new blood vessels were observed (Figs. 6C1-C6). The E2 group showed active bone remodeling with the thickest and most compact new bone formation being in the defect area compared to that of other groups. Increased osteophytic bone formation was observed. Furthermore, an increased number of Haversian canals with osteoblast rimming and new blood vessel formation stained with thick red color by the MT stain were seen (Figs. 6D1-D6).

We counted the number of osteocytes and Haversian canals in the ROI for quantitative analysis. The results showed that the E2 groups had a statistically significant greater osteocyte count compared to the control groups ($p < 0.05$) (Table 7).

In order to confirm the inflammatory, angiogenic, and osteogenic properties in the control and experimental groups, IHC staining was performed. The expression of inflammation-related antibody IL-6 in the E2 group was weak (score “2”: 1–25% of cells positive), compared with that of the C1 group (“5”: 76–100% cells stained). TGF-β1 expression was markedly high in the E1 group, while the C1 group showed no expression (“1”: none). The TNF-α antibody stained strongly in the C1 and C2 groups compared to that in the other groups (“5”: 76–100% cells stained).

The expression of VEGF-A was the highest (“5”: 76–100%) compared to that of E2 (“2”: 1–25%). The osteogenesis markers, ALP and OPN, were also strongly expressed in the E1 group compared to that seen in other groups (Fig. 7).

4. Discussion

The standard regimen for jaw OM treatment has been well established in the scientific literature, which consists of early diagnosis, elimination of infection source, establishment of surgical drainage, bacteriological identification, antibiotic therapy, surgical treatment, supportive treatment, and lastly

reconstruction[16]. There are a variety of conventional treatment options that include antibiotics, nonsteroidal anti-inflammatory drugs, and hyperbaric oxygen therapy that is used as an adjunctive treatment, but the disease still has a high recurrence rate and life-threatening complications[1,17,18]. Therefore, it is important to establish an effective treatment method for jaw OM.

In the oral and maxillofacial surgery field, evidence suggests that active and passive decompression promotes osteogenesis, stimulates angiogenesis, creates short-term hypoxia, and exerts forces capable of removing the cystic lining and its contents as a definitive treatment for odontogenic cysts of the jaw[7]. According to an observational study by Lin *et al.*, negative pressure drainage for oral and maxillofacial surgery patients found that its application can hasten wound healing, decrease hospital stay length, improve patient comfort, and decrease clinician workload[19]. Also, an animal study by Zhang *et al.* found that intermittent negative pressure reduced bone healing time and enhanced bone regeneration by enhancing the expression of VEGF and bone morphogenetic protein 2[20]. Nakahashi *et al.* reported that closed continuous irrigation-suction treatment was effective not only for chronic suppurative jaw OM but also for the more intractable sclerosing type of OM after following complete removal of the affected tissues[21]. Based on our current animal study and previous reports, decompression effects with drainage have several important therapeutic effects including reduced treatment time, enhanced bone regeneration, and reduced complication and recurrence rates.

The significance of this study is that it demonstrates the effectiveness of decompression using a drain in jaw OM, which had significant bone healing effects according to micro-CT, histology, and IHC analyses. For developing new therapeutic methods for OM of the jaw, it is important to establish standard operative protocols for animal modeling[22]. To our knowledge, there are no scientific data in the literature on decompression effects using drain in jaw OM animal model. Also, the current *S. aureus*-infected jaw osteomyelitis rat model has not been previously described in the literature before.

The mechanisms of decompression and drainage in bone healing can be explained by fluid removal and alteration of the wound environment to be conducive to healing. Excess fluid build-up is regarded as one of the major factors that compromise healing, partly owing to the compressive pressure that it exerts on local cells and surrounding tissue. Each cell has an intrinsic tension exerted by the interactions between its cytoskeleton and the extracellular matrix, that induce a proliferative response. If the fluid pressure is elevated in the interstitium, the proliferative response diminishes due to dampened intrinsic tension buildup. The fluid from the extracellular space is thought to communicate with the wound surface. Applying decompression and drainage to this area permits fluid removal from the extracellular space[23]. The removal of postoperative fluid allows decompression of the microvasculature that permits tissue perfusion by reducing pressure and enhancing blood circulation to the area. It will also remove the toxins, inflammatory exudate, and pathogenic bacteria from the operative site, which is considered to be an important element in the wound healing process.

Micro-CT analysis tools provided highly reproducible methodology with qualitative and quantitative assessment of bone microstructure. Micro-CT is considered to be a gold standard method for assessing

mineral density, bone morphology, and bone micro-architecture under various pathologic conditions[24,25]. We report our methodology according to the guidelines for assessment of bone microstructure in rodents using micro-CT[26] and results by following morphometric indices that can determine new bone formation[27]. The most informative parameters which show the course of bone healing are BV, BV/VOI, BS/BV, and BMD[25,27]. The BV/VOI in the E2 group showed a mean value of 11.44 ± 2.68 %, indicating the highest amount of bone regeneration that was significantly higher than that seen in the control groups. The Tb.N was the highest in the E2 group at 3.18 ± 1.101/mm, while the Tb/Sp was lowest among all the other groups at 0.13 ± 0.06 mm, indicating more bone closure. The volume of mineralized bone tissue was the highest in the E2 group at 0.73 ± 0.16 mm^3, which was significantly higher than that seen in the control groups. Bone healing is characterized by a gradual increase in BV, BMD, and a decrease in BS/BV, and the volume of pore space. The E1 and E2 groups had the highest values for BV and BMD, and a decreased value for BS/BV. The 3D evaluation showed more rapid bone healing was detected in the E1 and E2 groups compared to that of the positive control group C2 (Fig. 8). Micro-CT analysis showed more favorable outcomes in bone healing after decompression treatment.

In terms of bone healing and anti-inflammation, the experimental groups showed more effective results that included rapid bone healing, blood vessel formation, and reduced inflammation. The E2 group also had the highest osteocyte count. An increase in osteocytes plays a pivotal role in regulating bone turnover, which also enhances osteogenesis of stem cells, suggesting an important role in tissue regeneration[28]. The histological results suggested the most optimal bony healing was seen in the experimental groups, which is in accordance with the micro-CT analysis.

VEGF-A is thought to play an important role in regulating angiogenesis as well as bone development and regeneration. Angiogenesis and osteogenesis are two intimately connected processes that must be closely coupled to permit physiological bone function. In fact, alterations in vascular growth can alter the physiological bone healing process, which may lead to osteoporosis, osteonecrosis, and non-union fractures[29]. According to a previous clinical study, decompression had a direct influence on the microvascular circulation, and enhanced VEGF protein in the first day following surgical treatment, thereby activating osteogenesis-related proteins such as OPN and ALP was decreased on the second day[30]. In our study we demonstrated that VEGF was activated and reduced in the E2 group, leading to enhanced and accelerated bone healing compared to the E1 group, while bone healing was evident, but much slower.

In the bone remodeling phase, TNF-α and other pro-inflammatory cytokines are thought to play an important role in bone healing[31]. IL-6 is a well-known cytokine that stimulate osteoclast differentiation and bone resorption indirectly depending on the context of release[32]. TNF-α is a widely known key player in the pathogenesis of osteomyelitis. Yokota *et al.* reported that the combination of IL-6 and TNF-α differentiated tartrate-resistant acid phosphatase-positive multinucleated cells, that resembles bone-resorbing cells. There osteoclast-like cells are easily inhibited by extracellular signal-regulated kinase unlike the osteoclasts. Therefore, these cells can be called as “inflammatory osteoclast like cells”[33]. In

IHC staining, the pro-inflammatory antibodies IL-6 and TNF-α were strongly stained in the C1 group, indicating an inflammatory reaction to the bacteria, while the groups which received surgical treatment were weakly stained. From the Micro-CT and histology analysis, C1 and C2 groups exhibited the weakest bone healing with strong inflammatory infiltration, which could be explained by the high expression of IL-6 found in C1, and high expression of TNF-α in the C1 and C2 groups. The high expression of IL-6 and TNF-α found in these groups had active bone resorptive effects, which suppressed the osteogenesis.

TGF-β is an important cytokine that balances bone formation and bone resorption, mineral storage, hematopoietic cell generation and osteoimmunology[34,35]. In the immune system, TGF-β modulates inflammatory responses by regulation of chemotaxis, activation and survival of macrophages, natural killer cells, mast cells, granulocytes and dendritic cells[35]. Especially, high concentration of TGF-β1 reduces the activation of osteoclasts, while low concentrations promotes osteoclast maturation[36]. The TGF-β1 was expressed in high expression in the E1 group. Previous studies suggest that TGF-β1 prevents TNF-α-induced bone destruction by suppressing effecter T cell function[35]. TGF-β1 also play an important role in vasculogenesis, induced by VEGF-mediated apoptosis[37]. The high expression of TGF-β1 found in the E1 group indicate active angiogenic function of decompression as well reduced activation of osteoclasts and bone resorption. Compared to E1 group, the E2 group showed well-formed cortical bone with less marrow bone. This could also explain the weak stain of angiogenesis and osteogenesis related antibodies, since adequate and compact bone healing was already established compared to that of other groups.

The results were in accordance with our hypothesis that decompression using a drain had significant therapeutic effects on bone regeneration for jaw OM. When decompression was applied to the curettage treatment, enhanced wound and bone healing were achieved. The decompression effects on the healing process were much enhanced with weekly normal saline irrigation.

Therefore, it could be recommended to implement decompression using a drain as a treatment in combination with surgical treatment to allow accelerated bone healing.

Declarations

Compliance with Ethical Standards

- This study had no funding.

- There are no conflicts of interest in this article

- Ethical approval: The experimental protocols were approved by the Seoul National University (SNU) Institutional Animal Care and Use Committee (SNU-121123-12-11) and Institutional Biosafety Committee of SNU (SNUIBC-R121226-1-6). The experiment was in accordance with the “Recommendations for handling of Laboratory Animals for Biomedical Research” and complied with the Committee on Safety and ethical Handling Regulations for Laboratory Experiments at SNU. Animal studies were conducted

following the ARRIVE guidelines and are in accordance with the 1964 Helsinki declaration and its later amendments or comparable ethical standards.

Data availability

- The datasets generated during and/or analyzed by the authors during this study are available from the corresponding author on reasonable request.

References

1 Chen, L. *et al.* Risk factors of recurrence and life-threatening complications for patients hospitalized with chronic suppurative osteomyelitis of the jaw. *BMC Infect Dis***13**, 313, doi:10.1186/1471-2334-13-313 (2013).

2 Cassat, J. E. & Skaar, E. P. Recent advances in experimental models of osteomyelitis. *Expert Rev Anti Infect Ther***11**, 1263-1265, doi:10.1586/14787210.2013.858600 (2013).

3 Dym, H. & Zeidan, J. Microbiology of acute and chronic osteomyelitis and antibiotic treatment. *Dent Clin North Am***61**, 271-282, doi:https://doi.org/10.1016/j.cden.2016.12.001 (2017).

4 Gudmundsson, T., Torkov, P. & Thygesen, T. Diagnosis and treatment of osteomyelitis of the jaw – a systematic review (2002-2015) of the literature. *J Dent & Oral Disord***3**, 1066 (2017).

5 Kim, S. G. & Jang, H. S. Treatment of chronic osteomyelitis in Korea. *Oral Surg Oral Med Oral Pathol Oral Radiol Endod***92**, 394-398, doi:10.1067/moe.2001.117810 (2001).

6 Baltensperger, M. & Eyrich, G. in *Osteomyelitis of the jaws* (eds Marc M. Baltensperger & Gerold K. H. Eyrich) 5-56 (Springer Berlin Heidelberg, 2009).

7 Castro-Núñez, J. Distraction sugosteogenesis: its biologic bases and therapeutic principles. *J Craniofac Surg***29**, 2088-2095, doi:10.1097/scs.0000000000004892 (2018).

8 Flynn, T. R., Hoekstra, C. W. & Lawrence, F. R. The use of drains in oral and maxillofacial surgery: a review and a new approach. *J Oral Maxillofac Surg***41**, 508-511, doi:10.1016/0278-2391(83)90241-0 (1983).

9 Qiu, Y. *et al.* Therapeutic efficacy of vacuum sealing drainage-assisted irrigation in patients with severe multiple-space infections in the oral, maxillofacial, and cervical regions. *J Craniomaxillofac Surg***47**, 837-841, doi:10.1016/j.jcms.2019.01.031 (2019).

10 Percie du Sert, N. *et al.* The ARRIVE guidelines 2.0: Updated guidelines for reporting animal research. *PLoS Biol***18**, e3000410, doi:10.1371/journal.pbio.3000410 (2020).

11 Fukushima, N., Yokoyama, K., Sasahara, T., Dobashi, Y. & Itoman, M. Establishment of rat model of acute staphylococcal osteomyelitis: relationship between inoculation dose and development of osteomyelitis. *Arch Orthop Trauma Surg***125**, 169-176, doi:10.1007/s00402-004-0785-z (2005).

12 An, Y. H., Kang, Q. K. & Arciola, C. R. Animal models of osteomyelitis. *Int J Artif Organs***29**, 407-420, doi:10.1177/039139880602900411 (2006).

13 Dong, Q. N., Kanno, T., Bai, Y., Sha, J. & Hideshima, K. Bone regeneration potential of uncalcined and unsintered hydroxyapatite/poly l-lactide bioactive/osteoconductive sheet used for maxillofacial reconstructive surgery: An in vivo study. *Materials (Basel)***12**, 2931, doi:10.3390/ma12182931 (2019).

14 Meyerholz, D. K. & Beck, A. P. Principles and approaches for reproducible scoring of tissue stains in research. *Lab. Invest.***98**, 844-855, doi:10.1038/s41374-018-0057-0 (2018).

15 Zhang, B. *et al.* Expression and distribution of SIBLING proteins in the predentin/dentin and mandible of hyp mice. *Oral Dis***16**, 453-464, doi:10.1111/j.1601-0825.2010.01656.x (2010).

16 Koorbusch, G. F., Deatherage, J. R. & Curé, J. How can we diagnose and treat osteomyelitis of the jaws as early as possible? *Oral Maxillofac Surg Clin North Am***23 4**, 557-567 (2011).

17 Urade, M., Noguchi, K., Takaoka, K., Moridera, K. & Kishimoto, H. Diffuse sclerosing osteomyelitis of the mandible successfully treated with pamidronate: a long-term follow-up report. *Oral Surg Oral Med Oral Pathol Oral Radiol***114**, e9-e12, doi:https://doi.org/10.1016/j.oooo.2012.02.017 (2012).

18 Kim, S. M., Woo, K. M., Myoung, H., Lee, J. H. & Lee, S. K. Tissue engineering treatment in osteomyelitis of the jaws. *Tissue Eng Regen Med***12**, 11-26, doi:10.1007/s13770-013-0414-4 (2015).

19 Lin, Y., Wang, H. & Zhang, X. Application of vacuum sealing drainage in oral and maxillofacial surgery. *Biomed Res***29**, 628-632 (2018).

20 Zhang, Y.-g. *et al.* Negative pressure technology enhances bone regeneration in rabbit skull defects. *BMC Musculoskelet Disord***14**, 76, doi:10.1186/1471-2474-14-76 (2013).

21 Nakahashi, K. *et al.* Closed continuous irrigation-suction treatment for chronic osteomyelitis of the mandible. *Int. J. Oral Maxillofac. Surg.***26**, 147, doi:10.1016/S0901-5027(97)81288-X (1997).

22 Kim, J.-H. & Kim, H.-W. Rat defect models for bone grafts and tissue engineered bone constructs. *Tissue Eng Regen Med***10**, 310-316, doi:10.1007/s13770-013-1093-x (2013).

23 Huang, C., Leavitt, T., Bayer, L. R. & Orgill, D. P. Effect of negative pressure wound therapy on wound healing. *Curr Probl Surg***51**, 301-331, doi:10.1067/j.cpsurg.2014.04.001 (2014).

24 Faot, F., Chatterjee, M., de Camargos, G. V., Duyck, J. & Vandamme, K. Micro-CT analysis of the rodent jaw bone micro-architecture: A systematic review. *Bone Rep.***2**, 14-24,

doi:https://doi.org/10.1016/j.bonr.2014.10.005 (2015).

25 Kustro, T. *et al.* Quantification of the mandibular defect healing by micro-CT morphometric analysis in rats. *J Craniomaxillofac Surg***46**, 2203-2213, doi:https://doi.org/10.1016/j.jcms.2018.09.022 (2018).

26 Bouxsein, M. L. *et al.* Guidelines for assessment of bone microstructure in rodents using micro-computed tomography. *J Bone Miner Res***25**, 1468-1486, doi:10.1002/jbmr.141 (2010).

27 Kallai, I. *et al.* Microcomputed tomography–based structural analysis of various bone tissue regeneration models. *Nat. Protoc***6**, 105-110, doi:10.1038/nprot.2010.180 (2011).

28 Cao, W. *et al.* Is there a governing role of osteocytes in bone tissue regeneration? *Curr Osteoporos Rep.***18**, 541-550, doi:10.1007/s11914-020-00610-6 (2020).

29 Grosso, A. *et al.* It takes two to tango: coupling of angiogenesis and osteogenesis for bone regeneration. *Front Bioeng Biotechnol***5**, doi:10.3389/fbioe.2017.00068 (2017).

30 Kim, S. M., Eo, M. Y., Cho, Y. J., Kim, Y. S. & Lee, S. K. Immunoprecipitation high performance liquid chromatographic analysis of healing process in chronic suppurative osteomyelitis of the jaw. *J Craniomaxillofac Surg* **46**, 119-127, doi:https://doi.org/10.1016/j.jcms.2017.10.017 (2018).

31 Mountziaris, P. M. & Mikos, A. G. Modulation of the inflammatory response for enhanced bone tissue regeneration. *Tissue Eng Part B Rev***14**, 179-186, doi:10.1089/ten.teb.2008.0038 (2008).

32 Blanchard, F., Duplomb, L., Baud'huin, M. & Brounais, B. The dual role of IL-6-type cytokines on bone remodeling and bone tumors. *Cytokine Growth Factor Rev***20**, 19-28, doi:10.1016/j.cytogfr.2008.11.004 (2009).

33 Yokota, K. *et al.* Combination of tumor necrosis factor α and interleukin-6 induces mouse osteoclast-like cells with bone resorption activity both in vitro and in vivo. *Arthritis Rheumatol***66**, 121-129, doi:10.1002/art.38218 (2014).

34 Wu, M., Chen, G. & Li, Y.-P. TGF-β and BMP signaling in osteoblast, skeletal development, and bone formation, homeostasis and disease. *Bone Research***4**, 16009, doi:10.1038/boneres.2016.9 (2016).

35 Kasagi, S. & Chen, W. TGF-beta1 on osteoimmunology and the bone component cells. *Cell Biosci***3**, 4-4, doi:10.1186/2045-3701-3-4 (2013).

36 Dieudonné, S. C., Foo, P., van Zoelen, E. J. & Burger, E. H. Inhibiting and stimulating effects of TGF-beta 1 on osteoclastic bone resorption in fetal mouse bone organ cultures. *J Bone Miner Res***6**, 479-487, doi:10.1002/jbmr.5650060509 (1991).

37 Ferrari, G., Cook, B. D., Terushkin, V., Pintucci, G. & Mignatti, P. Transforming growth factor-beta 1 (TGF-beta1) induces angiogenesis through vascular endothelial growth factor (VEGF)-mediated apoptosis. *J Cell Physiol* **219**, 449-458, doi:10.1002/jcp.21706 (2009).

Figures

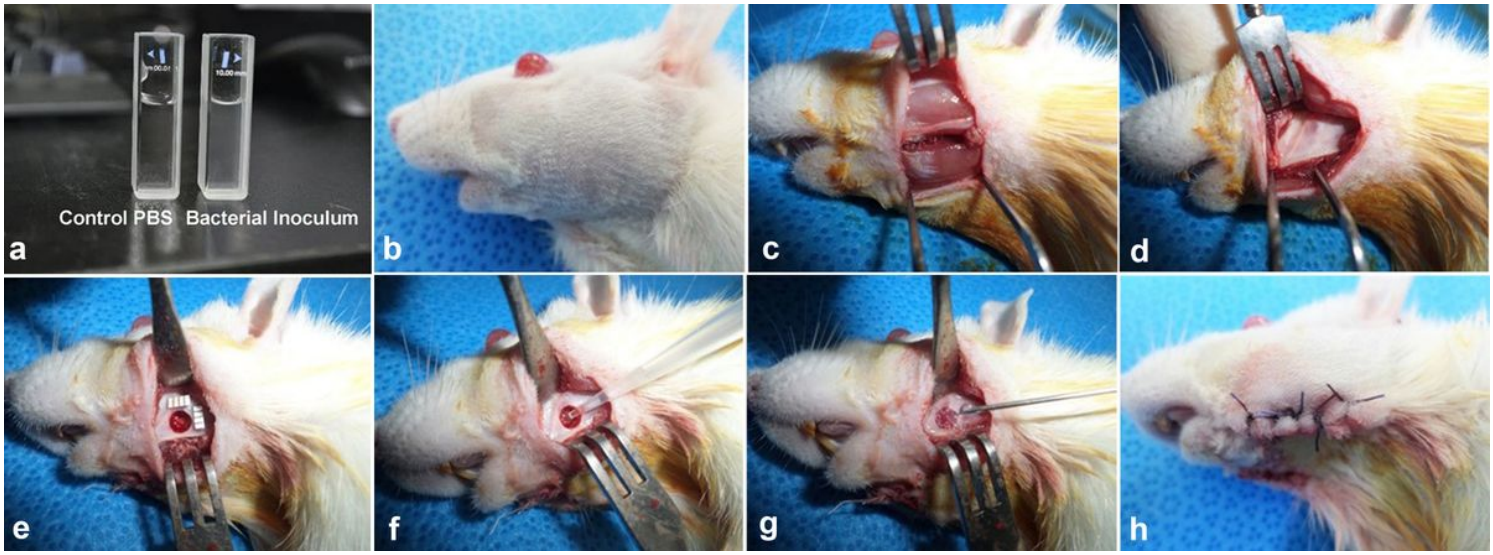

Figure 1

A UV/VIS spectrophotometer (Spectrophotometer, PerkinElmer®, MA, USA) adjusted to 0.8 OD at 600 nm was used to measure the bacterial density for infection (A). The preparations for the surgical procedure including the skin preparation, disinfection, and draping were all performed according to standard protocols (B). An approximately 12 mm full-thickness longitudinal extra-oral incision was made parallel to the inferior border of the right and left side of rat mandibles. Adequate subcutaneous (C), deep fascial and periosteal dissections were performed followed by retraction with forceps (D). Using a low-speed hand piece with 1.2 mm diameter round bur, a bilateral circular 4 mm defect was created in the rat mandible (E) with copious irrigation. All animals received 20 µl of 107 CFU/ml S. aureus injection (F) into the defect and were covered with Greenplast kit® fibrin glue (Greencross Co., Yongin, Korea) (G). The surgical wound was then carefully sutured at the subcutaneous layer with resorbable 4-0 Vicryl® (Polyglactin 910®, Johnson & Johnson Co., NJ, USA) sutures and the skin closure was performed using silk sutures (Black silk®, 2–0; AILEE Co., Busan, Korea) (H).

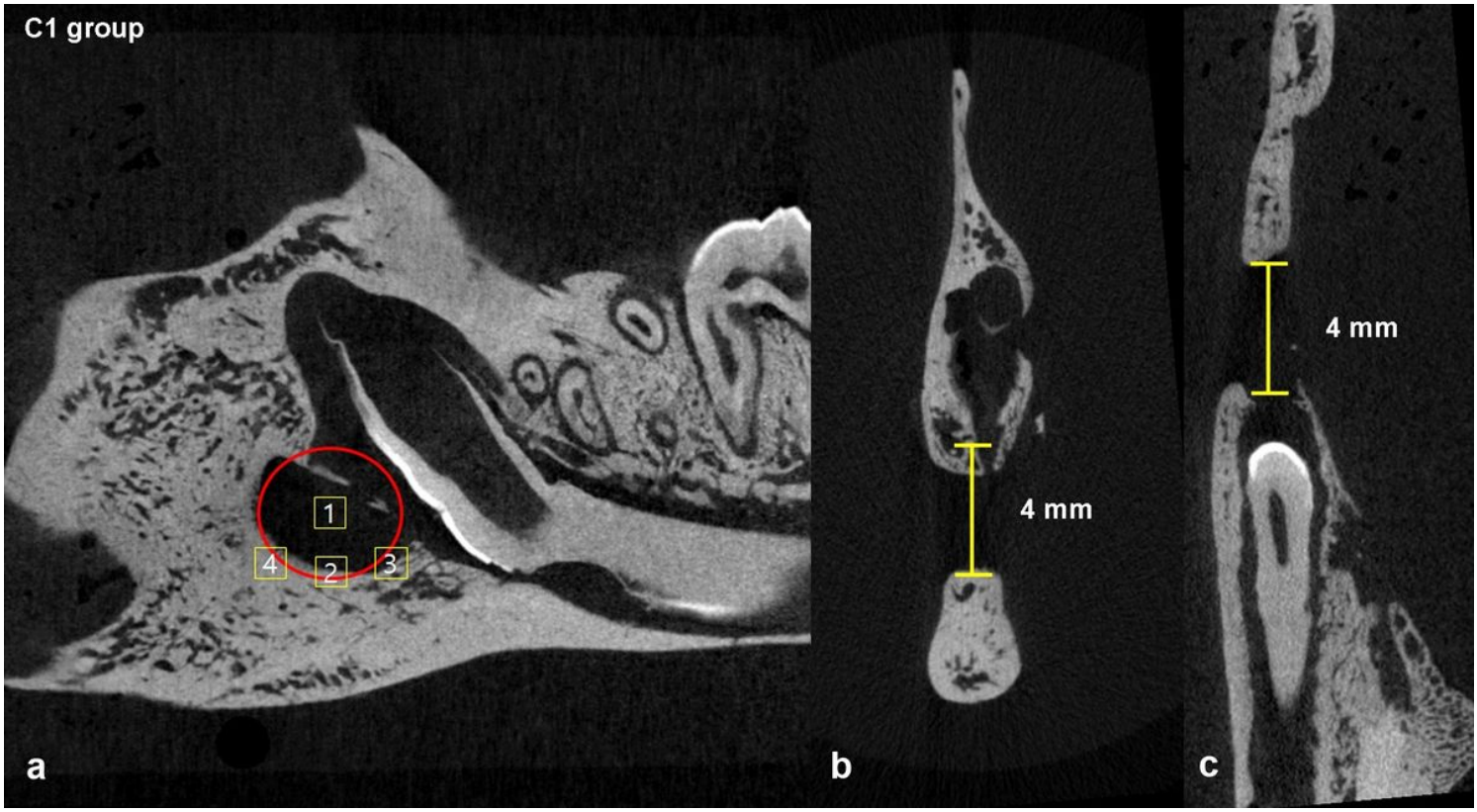

Figure 2

ROI designation method at the round 4 mm defect area. A circular area with a 4 mm wide diameter was first set in the sagittal plane that depicted the defect and four 1 x 1 mm square ROIs were set at the center of the defect and the inferior margins of the circular area (A). Axial plane showing bone defects and bone destruction at the buccal surface of the rat mandible (B). Coronal view showing the bone defect marked with yellow color (C).

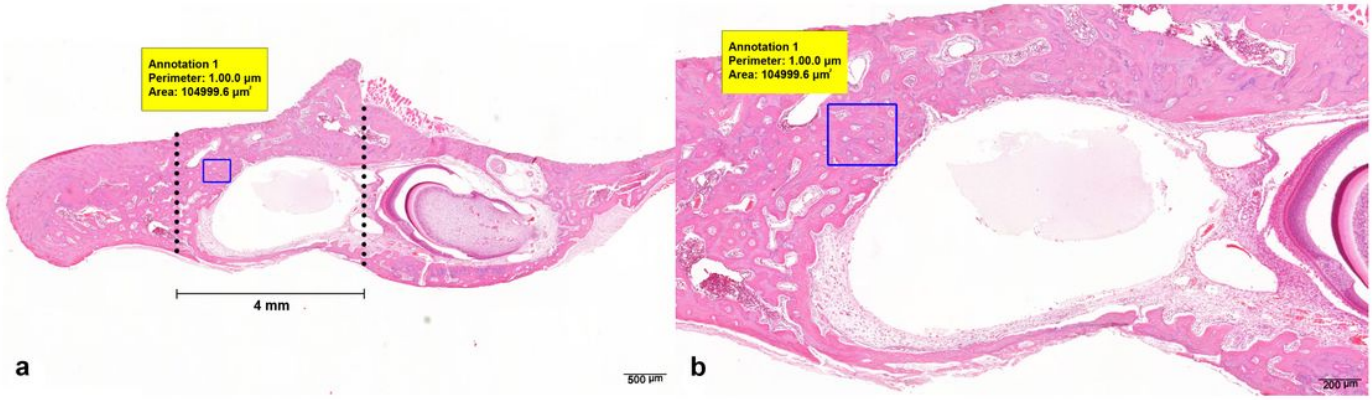

Figure 3

Osteocyte and Haversian canal count method, 2x (A). At the center of the defect area with bone regeneration, a 500 x 500 µm fixed rectangle was selected as the area of interest for counting, 5x (B).

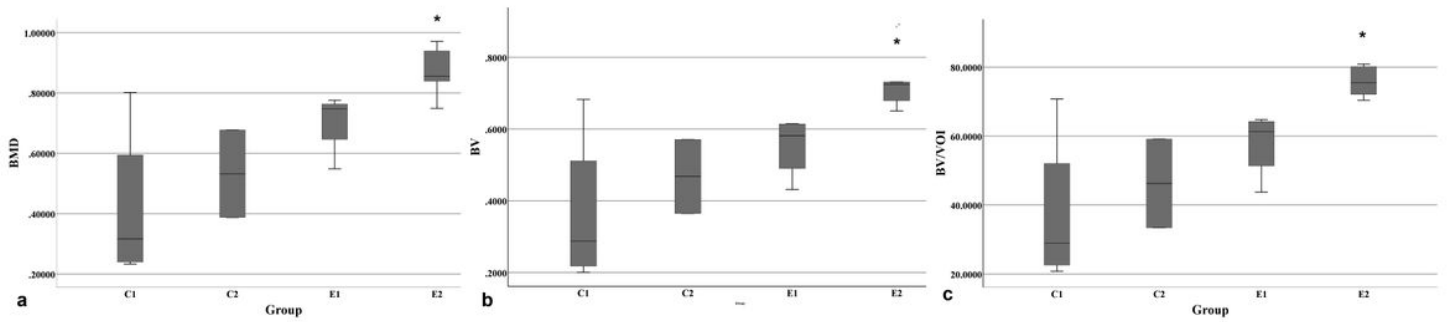

Figure 4

BMD differences between the groups. The E2 group was significantly higher than the C1 group (*p< 0.05) (A). The BV and BV/VOI was significantly higher in the E2 group than in the control groups (*p< 0.05), while the E1 group showed no significant differences with other groups (B-C).

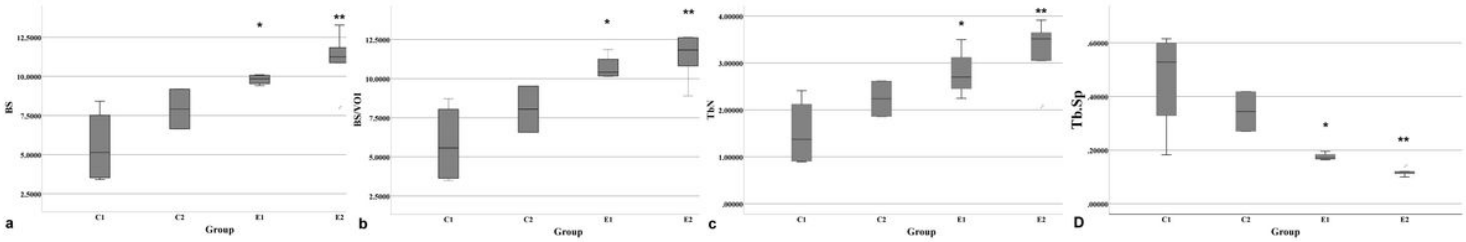

Figure 5

Comparison of micro-CT parameters between the groups. BS (A), bone surface and BS/VOI (B), Tb.N (C), Tb.Sp (D) (*, **p< 0.05).

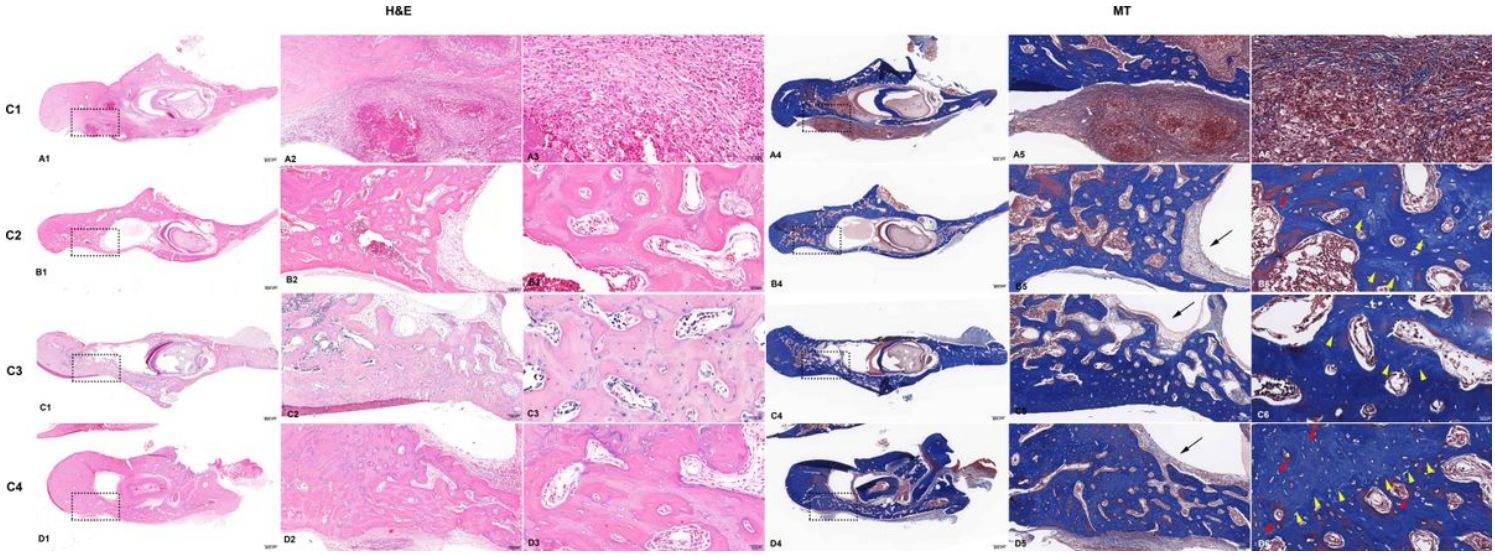

Figure 6

Representative histological images of the specimens following 4 weeks of treatment stained with H&E and MT. In the C1 group, intense inflammatory infiltration is observed, 5.0x (A1). Magnification of the

rectangles, 10x, 40x (A2-A3). MT stain for bone regeneration in the defect area (A4). Magnification of the rectangles, 10x, 40x (A5-A6). The C2 group showed bone healing with osteoblastic cell lining in the parenchymal tissue found at the center of the defect area with evidence of inflammatory infiltrates (B1). Magnification of the rectangles, 10x, 40x (B2-B3). MT stain for bone regeneration in the C2 group at 2x (B4). Magnification of the rectangles, 10x, 40x (B5-B6). The E1 group showed loose marrow fibrosis and scattered lymphocytic inflammatory infiltrates (C1). High power view of the rectangles, 10x, 40x (C2-C3). The MT stain of E1 group showed new bone formation stained with bright blue color and new blood vessels were observed (C4). Magnification of the rectangles, 10x, 40x (C5-C6). The E2 group showed increased osteophytic bone formation (D1). High power view of the rectangles at 10x, 40x (D2-D3). The E2 group showed active bone remodeling with the thickest compact new bone formation in the defect area compared to that of other groups (D4). An increased number of Haversian canals with osteoblast rimming and new blood vessel formation stained with thick red color by the MT stain were observed at 10x, 40x magnification (D5-D6). Black arrow, parenchymal tissue, Yellow arrowhead, new bone formation, Red arrow, blood vessel formation.

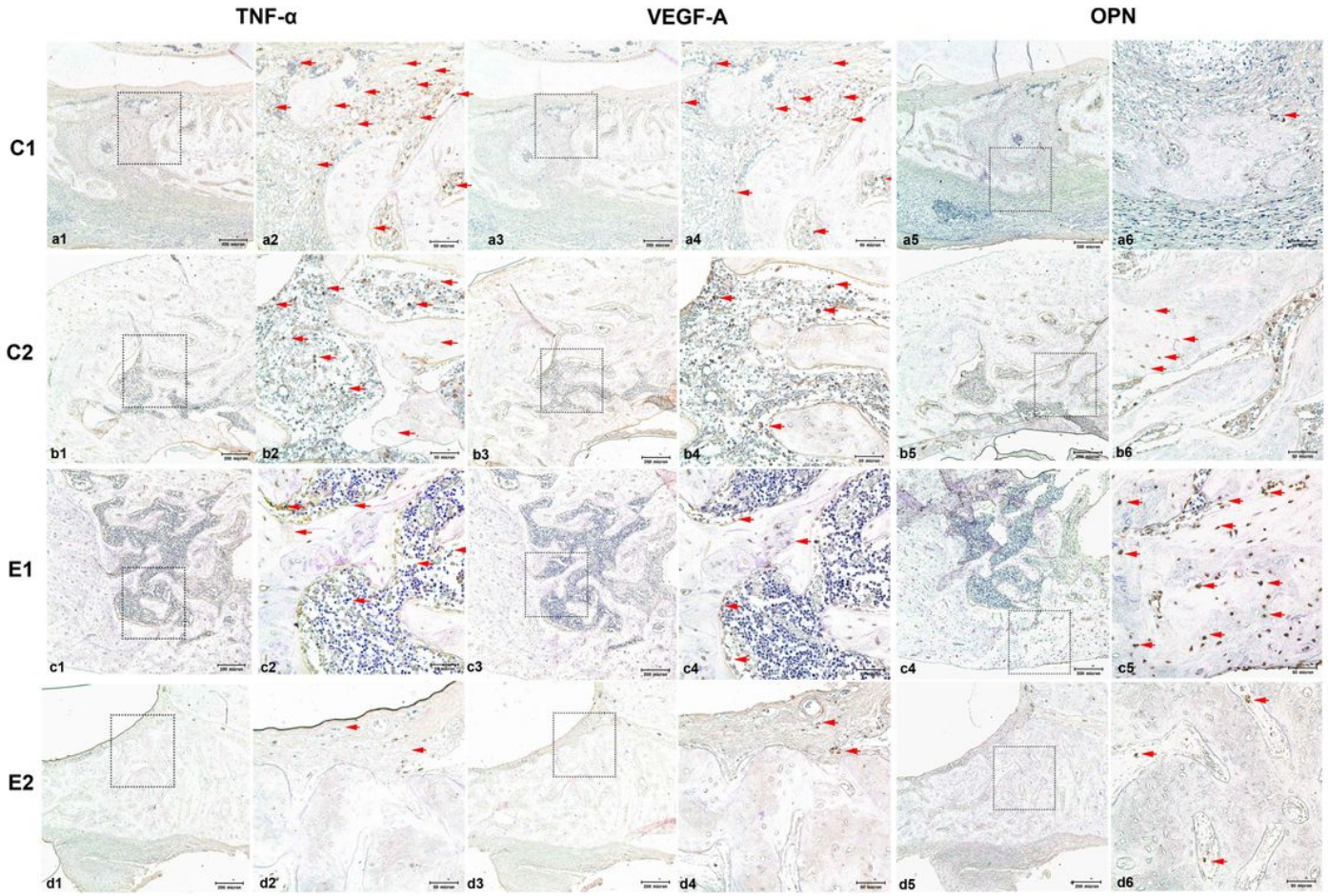

Figure 7

TNF-α, VEGF-A, and OPN antibody staining in the C1 group (A), C2 group (B), E1 group (C), and E2 group (D). TNF-α staining with original magnification, 10x (A1), Magnified image from the selected region from a1, 40x (A2). VEGF-A staining with original magnification, 10x (A3), Magnified image from the selected region from a1, 40x (A4). OPN staining with original magnification, 10x (A5), Magnified image from the selected region from a1, 40x (A6). The red arrowheads mark the stained antibodies in the defect area.

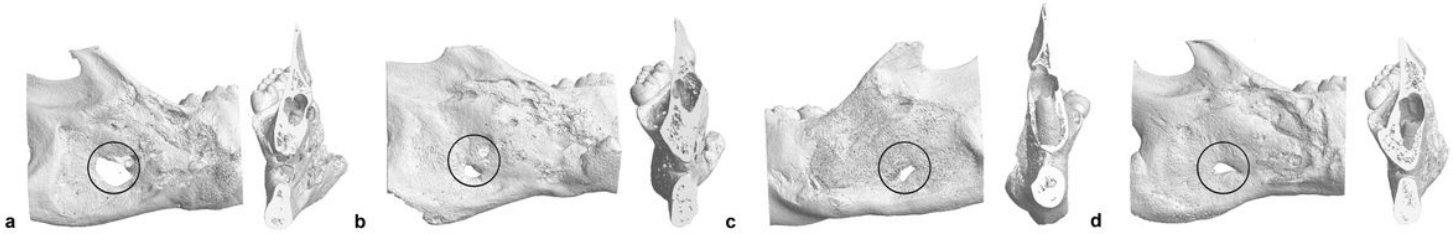

Figure 8

3D reconstructed images of the C1 (A), C2 (B), E1 (C), and E2 (D) groups. Images show the enhanced bone healing in the round defect in the E1 and E2 groups.